Dalton Transactions

Accepted Manuscript

ROYAL SOCIETY OF CHEMISTRY

www.rsc.org/dalton

For Table of contents use only

Iron(II) complexes featuring κ^3- and κ^2-bound PNP pincer ligands - The significance of sterics

A series of octahedral Fe(II) complexes of the type $[Fe(\kappa^3\text{-}P,N,P\text{-PNP})(\kappa^2\text{-}P,N\text{-PNP})X]^+$ (X = Cl, Br) where PNP pincer ligands are coordinated both in κ^3-*P,N,P*- and κ^2-*P,N*-fashion are prepared and characterized. All complexes undergo facile rearrangement reactions upon halide dissociation to give the dicationic complexes $[Fe(\kappa^3\text{-}P,N,P\text{-PNP})_2]^{2+}$ where both PNP ligands are bound in κ^3-*P,N,P*-fashion.

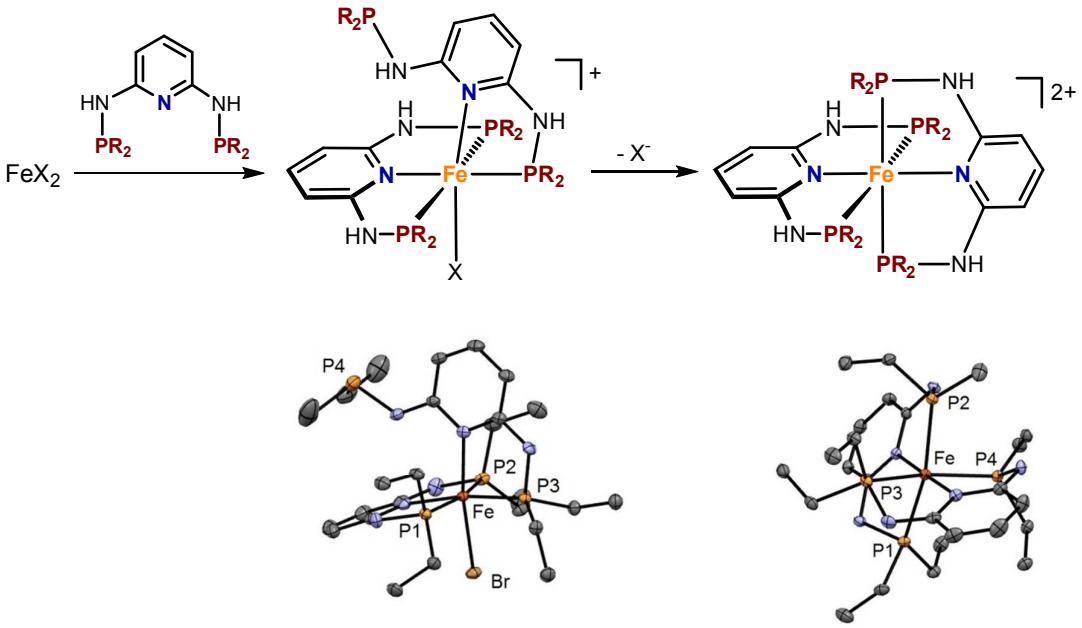

Iron(II) complexes featuring κ^3- and κ^2-bound PNP pincer ligands - The significance of sterics

Mathias Glatz,[a] Bernhard Bichler,[a] Matthias Mastalir,[a] Berthold Stöger,[b] Matthias Weil,[b] Kurt Mereiter,[b] Ernst Pittenauer,[b] Günter Allmaier,[b] Luis F. Veiros,[c] and Karl Kirchner*,[a]

Abstract

Treatment of anhydrous FeX_2 (X = Cl, Br) with 2 equivs of the sterically little demanding N,N'-bisphosphino-2,6-diaminopyridine based PNP ligands - featuring Ph, biphenol (BIPOL), Me, Et, *n*Pr, and *n*Bu substituents at the phosphorus sites and H, Me, and Ph substituents at the N-linkers - afforded diamagnetic cationic octahedral complexes of the general formula [Fe(κ^3-*P,N,P*-PNP)(κ^2-*P,N*-PNP)X]$^+$ featuring a κ^2-*P,N* bound PNP ligand. With the sterically more encumbered N-methylated ligand PNP^{Me}-Ph the related complex [Fe(κ^3-*P,N,P*-PNP^{Me}-Ph)(κ^2-*P,N*-PN^{HMe}-Ph)Cl]$^+$ rather than [Fe(κ^3-*P,N,P*-PNP^{Me}-Ph)Cl_2] was formed. This reaction was accompanied by P-N bond cleavage thereby forming the κ^2-*P,N*-bound N-diphenylphosphino-N,N'-methyl-2,6-diaminopyridine ligand. In contrast, with the N-phenylated ligand PNP^{Ph}-Et and PNP^{Ph}-*n*Pr, despite of small Et and *n*Pr substituents at the phosphorus sites, complexes [Fe(κ^3-*P,N,P*-PNP^{Ph}-Et)Cl_2] and [Fe(κ^3-*P,N,P*-PNP^{Ph}-*n*Pr)Cl_2] were formed revealing that sterics can be also controlled by substituent variations at the amino N-sites. Depending on the solvent, complexes featuring κ^2-*P,N*-bound ligands undergo facile rearrangement reactions to give dicationic complexes of the type [Fe(κ^3-*P,N,P*-PNP)$_2$]$^{2+}$ where both PNP ligands are bound in κ^3-*P,N,P*-fashion. In the presence of either Ag^+ or Na^+ salts as halide scavengers this reaction takes place within a few minutes. The pendant PR_2 arm of the κ^3-κ^2-complexes is readily oxidized to the corresponding phosphine sulfides upon treatment with elemental sulfur. This was exemplarily shown for [Fe(κ^3-*P,N,P*-PNP-*n*Pr)(κ^2-*P,N*-PNS-*n*Pr)Cl]$^+$. Halide abstraction afforded the dicationic bis-chelated octahedral Fe(II) complex [Fe(κ^3-*P,N,P*-PNP)$_2$]$^{2+}$ together with the free SNP ligand rather than [Fe(κ^3-*P,N,P*-PNP-*n*Pr)(κ^3-*S,P,N*-PNS-*n*Pr)]$^{2+}$.

[a] Institute of Applied Synthetic Chemistry, Vienna University of Technology, Getreidemarkt 9, A-1060 Vienna, AUSTRIA, e-mail: kkirch@mail.tuwien.ac.at

[b] Institute of Chemical Technologies and Analytics, Vienna University of Technology, Getreidemarkt 9, A-1060 Vienna, AUSTRIA

[c] Centro de Química Estrutural, Instituto Superior Técnico, Universidade de Lisboa, Av. Rovisco Pais No. 1, 1049-001 Lisboa, PORTUGAL

†Electronic supplementary information (ESI) available. Synthetic details of compounds **1e, 1f**, **2f**BPh$^{Me}_4$, **2g**BF_4, **2h**BF_4, **5d**BF_4, **5e**BF_4, and **5f**BF_4. CCDC 1005380 (**2e**BPh$^{Me}_4$), 1005381 (**2f**BPh$^{Me}_4$), 1005382 (**3**), 1005385 (**5a**Cl), 1005384 (**5b**CF_3SO_3), 1005387 (**5c**CF_3SO_3), 1005386 (**5d**BPh_4), and 1024076 (**5e**BF_4). For ESI and crystallographic data in CIF or other electronic format see DOI: xxxxxxx.

Introduction

Neutral pyridine-based ENE pincer ligands where E is a (hetero)donor atom are widely utilized in transition metal chemistry due to their combination of stability, activity and variability.[1] They typically enforce a *meridional* κ^3-*E,N,E* coordination mode provided that three coordination sites are accessible at the metal center. As iron ENE complexes are concerned, an important class of compounds are coordinatively unsaturated 16e high-spin square-pyramidal complexes of the type [Fe(ENE)X_2] (X = Cl, Br) obtained from Fe(II) halides with stoichiometric amounts of ENE ligands. Examples of prominent ENE ligands are bis(imino)pyridines (**I**),[2,3,4] bis(phosphinomethyl)pyridines (**II**), bis(amino)pyridines (**III**),[5,6,7] 6-phosphinomethyl-2,2'-bipyridines (**IV**),[8] bis(imidazolylidene) pyridines (**V**),[9] terpyridines (**VI**)[10] and bis(phosphinito)pyridines (**VII**)[11] as shown in Chart 1. In most cases bulky R substituents such as *i*Pr or *t*Bu are required to avoid the formation of bis-chelated dicationic low-spin complexes of the type [Fe(ENE)$_2$]$^{2+}$. Some of these [Fe(ENE)X_2] complexes turned out to be highly active catalysts for polymerization reactions or are valuable precursors for Fe(0) complexes which, for instance, are useful catalysts for hydrogenation[12] and hydrosilation[13] reactions.

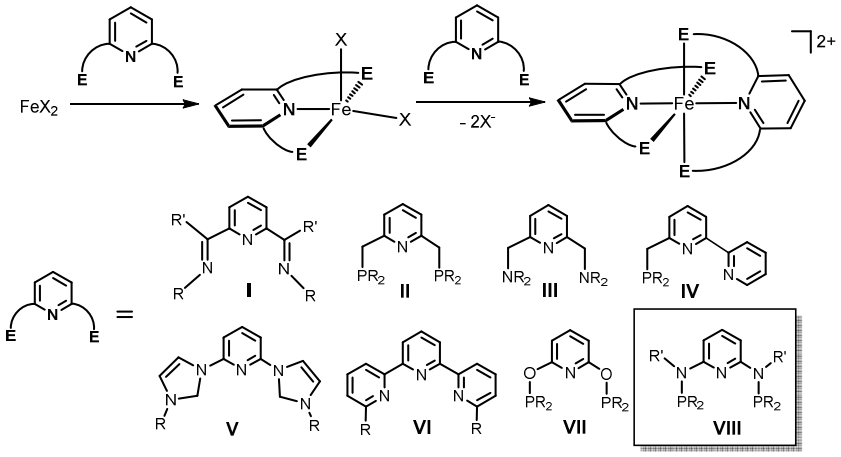

Chart 1

We are currently focusing on the synthesis and reactivity of iron complexes containing PNP pincer ligands based on the 2,6-diaminopyridine scaffold (**VIII**).[14] In these ligands the aromatic pyridine ring and the phosphine moieties are linked via NH, N-alkyl, or N-aryl linkers. In the course of our studies we discovered[14] that Fe(II) halides react with bulky PNP ligands N,N'-bis(di-*iso*-propylphosphino)-2,6-diaminopyridine (PNP-*i*Pr) and N,N'-bis(di-*tert*-butylphosphino)-2,6-diamino-pyridine (PNP-*t*Bu) to give the expected mono-chelated high-spin complexes [Fe(PNP)X_2], while with N,N'-bis(diphenylphosphino)-2,6-diaminopyridine (PNP-Ph) the *bis*-chelated octahedral Fe(II) complex [Fe(κ^3-*P,N,P*-PNP-Ph)(κ^2-*P,N*-PNP-Ph)Cl]$^+$ (**2a**)[15] was formed exclusively where the PNP pincer ligands are coordinated in κ^3-*P,N,P*- and κ^2-*P,N*-fashion (Scheme 1). These reactions were not sensitive to the ratio of the reactants. It has to be noted that the reaction of $FeCl_2$ with PNP^{CH2}-Ph

(chart 1, type **II**) yields the pentacoordinate complex [Fe(PNP^{CH2}-Ph)Cl$_2$] revealing striking differences between CH_2 and NH spacers in pyridine-based PNP pincer ligands (Scheme 1).

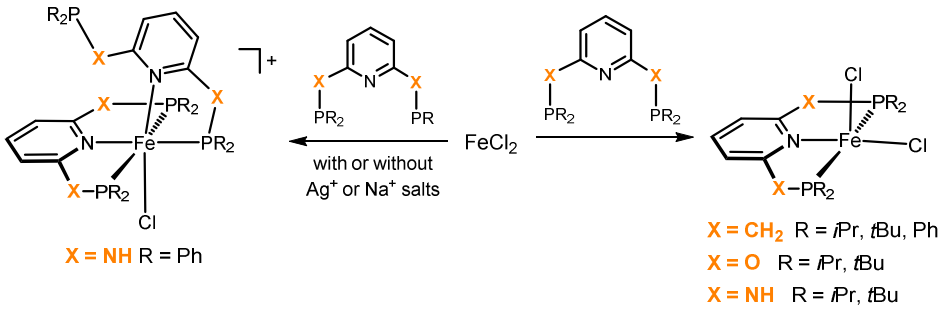

Scheme 1

In continuation of our studies on iron PNP complexes, we report here on the synthesis and reactivity of a series of octahedral Fe(II) complexes where PNP pincer ligands are coordinated in κ^3-*P,N,P*- and κ^2-*P,N*-fashion. In order to answer the question whether the formation of these complexes are sterically or electronically driven, we utilize PNP ligands with both weakly and strongly electron donating PR_2 substituents which, the exception of N-methylated and N-phenylated ligands, are sterically non-demanding (Chart 2). The bulkiness of these ligands, based on their cone angles estimated from crystallographic data[16,17,18] by the procedure of Mingos *et al.*,[19] decrease roughly in the order PNP^{Ph}-*n*Pr ≈ PNP^{Ph}-Et (120) > PNP^{Me}-Ph (105) > PNP-*n*Bu ≈ PNP-*n*Pr ≈ PNP-Et ≈ PNP-Ph (100) > PNP-BIPOL (95) > PNP-Me (90). For comparison, the cone angles of the previously reported PNP ligands PNP-*t*Bu, PNP^{Me}-*i*Pr, and PNP-*i*Pr are 130, 120, and 115, respectively.

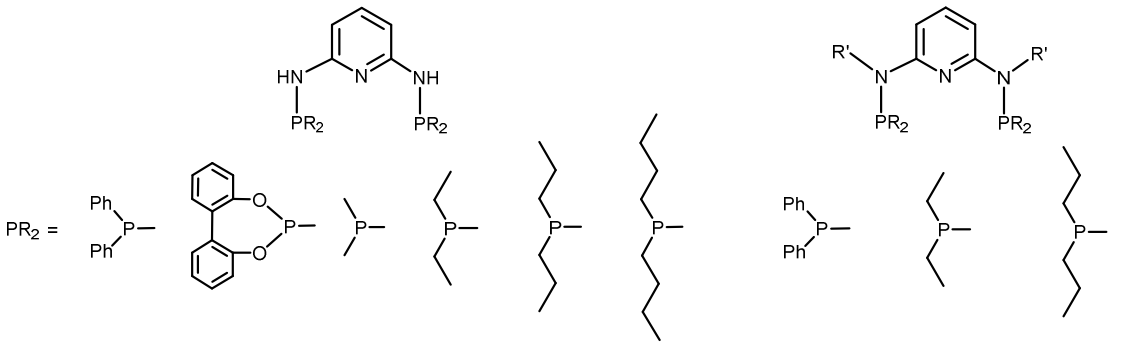

Chart 2

Results and Discussion

Synthesis of Fe(II) complexes featuring κ^3 and κ^2-bound PNP pincer ligands. Treatment of anhydrous $FeCl_2$ with 2 equivs of the ligands PNP-Ph (**1a**), PNP-BIPOL (**1b**), PNP-Me (**1c**), PNP-Et

(**1d**), PNP-*n*Pr (**1e**), and PNP-*n*Bu (**1f**) in THF at room temperature for 4h afforded diamagnetic emerald green cationic octahedral complexes of the general formula [Fe(κ^3-*P,N,P*-PNP)(κ^2-*P,N*-PNP)Cl]$^+$ (**2a-c**,**e**,**g**,**h**) in essentially quantitative yields (Scheme 2). The reaction of **1a** with $FeCl_2$ was described recently in a preliminary communication.[15] Analogous bromide complexes [Fe(κ^3-*P,N,P*-PNP)(κ^2-*P,N*-PNP)Br]$^+$ (**2d**,**f**) were obtained in similar fashion by straightforward complexation of the ligands **1c** and **1d** with anhydrous ferrous dibromide.

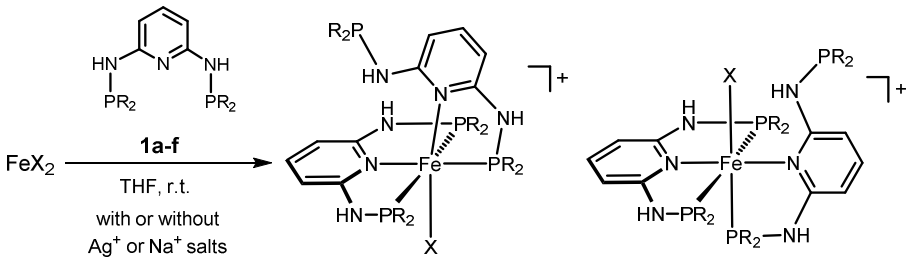

2a PNP-Ph, X = Cl
2b PNP-BIPOL, X = Cl
2c,d PNP-Me, X = Cl, Br
2e,f PNP-Et, X = Cl, Br
2g PNP-*n*Pr, X = Cl
2h PNP-*n*Bu, X = Cl

Scheme 2

The formation of these complexes is independent of whether 1 or 2 equivs of ligand are used. However, in the first case substantial amounts of unreacted FeX_2 remained which also form paramagnetic haloferrate counterions $[FeX_4]^{2-}$. All reactions are selective and the formation of only one isomer was observed where the pyridine moiety of the κ^2-*P,N* bound PNP ligand is *trans* to the halide ligand. With the exception of **2a** and **2b**, all complexes containing chloride and bromide counter ions were poorly soluble in most common solvents. In some cases, soluble, stable, and crystalline complexes were afforded upon counter ion exchange with halide scavengers such as $AgBF_4$ (**2a**), $Na\{B[C_6H_4\text{-}4\text{-}Me)_4\}$ ($NaBPh^{Me}_4$) (**2e**, **2f**), and $NaBF_4$ (**2g**, **2h**). However, in the case of **2b**, **2c**, and **2d** this procedure led to fast ligand rearrangement reactions (*vide infra*).

Most complexes were fully characterized by a combination of ^1H and $^{31}P\{^1H\}$ NMR spectroscopy, and elemental analysis. Complexes **2e**,**f**,**g**,**h** were also characterized by $^{13}C\{^1H\}$ NMR spectroscopy. The instability and poor solubility of **2c** and **2d** precluded the recording of NMR spectra. While the ^1H NMR spectra were not very informative, the $^{31}P\{^1H\}$ NMR spectra revealed in all cases an A_2B pattern for the κ^3- and κ^2 bound PNP ligands as well as a singlet for the pendant PR_2-NH-arm of the κ^2-bound PNP ligand.[20] Accordingly, in most cases $^{31}P\{^1H\}$ NMR chemical shifts and J_{PP} coupling constants had to be derived from simulations as exemplarily shown for **2g** in Figure 1.

Figure 1

DFT calculations (see Computational details) performed for complexes **2a, 2c**, and **2d** are in agreement with the experimental data indicating that the experientially observed isomer (denoted as **A**) is thermodynamically more stable by 6.9, 5.2, and 4.4 kcal/mol, respectively, than the unobserved isomer **B** (Figure 2). That stability difference is essentially due to steric effects, as shown in the space filling models for complexes **2a, 2c**, and **2d** in Figure 3 were it is clear that the ligand environment around the Cl ligand is more congested in isomer **B**.

Figures 2-3

Still in the case of complex **2a**, an indication for the stereochemical stress associated with **B** involving in particular the Cl ligand is the Cl-Fe-X angle, X being the atom *trans* to N_{py} of the κ^3-*P,N,P* bound PNP ligand. That angle is 88° in **A** and becomes 104° in **B** showing that the Cl ligand is considerably bent towards the κ^3-*P,N,P* bound PNP ligand in the latter species. This geometrical constraint has clear consequences in the bonding of the two isomers. Thus, the κ^3-*P,N,P* bound PNP ligand binds strongly to the metal in **B** in order to compensate the weakening of the coordination of the κ^2-*P,N* bound PNP ligand due to the repulsion with the Cl ligand in that molecule. This effect is clear in the Fe-N_{py} bond involving the κ^3-*P,N,P* bound PNP ligand which is weaker in **A** (d = 2.116 Å, WI = 0.27) than in **B** (d = 2.032 Å, WI = 0.37).[21] On the other hand, in the latter the Fe-N_{py} bond of the κ^2-*P,N* bound PNP ligand is much weaker with a distance of 2.198 Å. The Fe-Cl bond is also weaker in **B** as a result of the stereochemical repulsion. The Fe-Cl distance in **B** is 2.382 Å, compared with 2.376 Å in **A** and the difference in bond strength is even more evident in the corresponding Wiberg indices being 0.39 in **B** and 0.46 in **A**. The different coordination strength of the two PNP ligands in each complex is also reflected in the charges of those ligands. Accordingly, in **A** the overall charge (NPA, see Computational details) of the κ^3-PNP and κ^2-PNP ligands is 0.86 and 0.56, while in **B** these values are 0.89 and 0.49, respectively. This indicates that comparing **A** with **B** the κ^3-*P,N,P* bound PNP ligand becomes a stronger donor in **B** (more positive) while the opposite happens with the κ^2-*P,N* bound PNP ligand. It is interesting to note that the intramolecular H-bond does not explain the stability difference because it is actually stronger in the case of **B** (Cl···H-N) as can be seen, for example, by the N-H bonds (covalent) in both cases. That bond is weaker in the case of **B** (d = 1.027 Å) than in **A** (d = 1.015 Å) which is also apparent from the respective Wiberg indices for the H-bond being 0.02 for N···HN in **A**, and 0.09 for Cl···HN in **B**.

In an attempt to prevent the coordination of a second PNP ligand we utilized the N-methylated and N-phenylated ligands PNP^{Me}-Ph (**1g**), PNP^{Ph}-Et (**1h**) and PNP^{Ph}-*n*Pr (**1i**) assuming that κ^2-*P,N*-coordination of these ligands is highly unlikely due to unfavorable steric interactions with the pyridine unit of the κ^3-*P,N,P*-bound ligand. The reaction with two equivs of **1g** proceeded differently than expected yielding the cationic complex [Fe(κ^3-*P,N,P*-PNP^{Me}-Ph)(κ^2-*P,N*-PN^{HMe}-Ph)Cl]$^+$ (**3**) as shown in

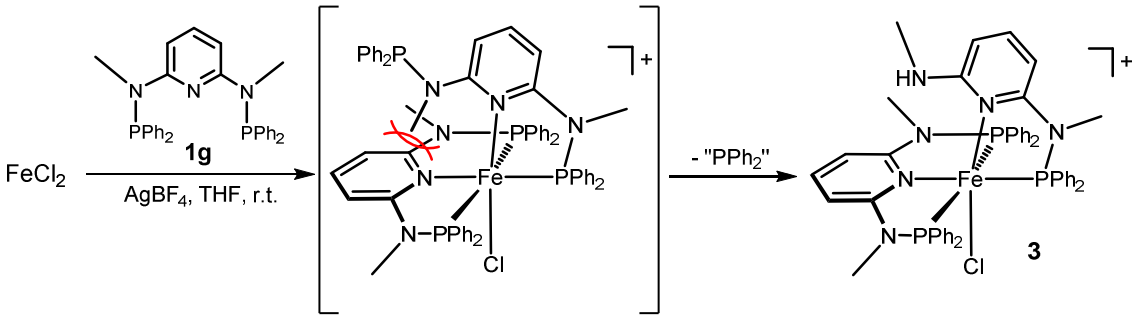

Scheme 3

Scheme 3. This reaction is accompanied by P-N bond cleavage thereby forming the new κ^2-*P,N*-bound N-diphenylphosphino-N,N'-methyl-2,6-diaminopyridine ligand. This reaction may be facilitated by adventitious water. The fate of the "PPh_2" moiety was not investigated but it is not uncommon that aminophosphines bearing phenyl substitutents at the phosphorous site are prone to hydrolysis forming for instance Ph_2POH.[22] On the other hand, treatment of anhydrous $FeCl_2$ with 1 or 2 equivs of **1h** and **1i** in THF at room temperature afforded the pentacoordinated high-spin complexes [Fe(PNP^{Ph}-Et)Cl_2] (**4a**) and [Fe(PNP^{Ph}-*n*Pr)Cl_2] (**4b**), respectively, in 97 and 95% isolated yields

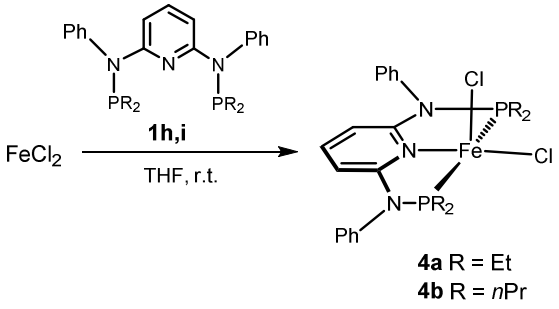

Scheme 4

(Scheme 4). This type of complexes is well established. At room temperature, solution magnetic moment measurements of complexes **4a** and **4b** in a CH_2Cl_2 solution was consistent with these complexes having four unpaired electrons (μ_{eff} = 4.9 and 4.8 μ_B, Evans' method). Accordingly, these complexes display large paramagnetic shifted and very broad ^{1}H NMR and $^{13}C\{^1H\}$ NMR signals and were thus not very informative. $^{31}P\{^1H\}$ NMR signals could not be detected.

The solid state structures of **2f**BPh$^{Me}_4$ and **3** determined by single-crystal X-ray diffraction are depicted in Figures 4 and 5 with selected bond distances given in the captions. The structure of **2e**BPh$^{Me}_4$ is provided in the ESI. The coordination geometry around the iron center of **2e**BPh$^{Me}_4$, **2f**BPh$^{Me}_4$, and **3** corresponds to a characteristically distorted octahedron agreeing well with that in the previously reported complex **2a**BF_4 of [Fe(κ^3-*P,N,P*-PNP-Ph)(κ^2-*P,N*-PNP-Ph)Cl]$BF_4\cdot$2THF$\cdot Et_2O$.[14] A view of the complex core of these four structures is shown in Figure 6 together with mean values and

ranges of selected geometric data. The bond lengths about iron are in narrow ranges irrespective whether there is an aryl- or an alkyl-PNP ligand. The Fe-P bonds of the κ^3-bonded ligand adopt normal values of 2.244 Å on average and are modestly longer than the bonds to the κ^2-bonded PNP ligand (mean value 2.186 Å). Likewise the Fe-N bonds to the pyridine nitrogen N1 of the κ^3-bonded ligand are systematically shorter than to N4 of the κ^2-bonded PNP ligand. The NH group (with N6) of the dangling arm of the κ^2-bonded PNP ligand is in all four complexes directed to the pyridine nitrogen N1 showing N6…N1 distances between 2.802 and 2.941 Å indicative for a stabilizing intramolecular hydrogen bond. This interaction is unusual because it seems to represent a hybrid between a classical N-H…N and an N-H…π interaction. This interaction is also responsible for that the pyridine ring of N1 is bent away from N6 so that the angle C3-N1-Fe (Figure 6) is about 170° whereas in normal κ^3-bonded Fe(PNP) complexes this angle is always very close to 180°.

Figures 4 - 6

Reactivity of Fe(II) complexes featuring κ^3 and κ^2-bound PNP pincer ligands. [Fe(κ^3-*P,N,P*-PNP-Ph)(κ^2-*P,N*-PNP-Ph)Cl]$^+$ (**2a**) is stable in THF for several days, but readily rearranges in CH_3CN (within a few minutes) and CH_2Cl_2 (within a few hours) to give [Fe(κ^3-*P,N,P*-PNP-Ph)$_2$]$^{2+}$ (**5a**). This process involves halide dissociation and a 90^o rotation of the κ^2-bound PNP ligand. In the presence of halide scavengers this reaction proceeds in all common solvents within a few minutes (Scheme 5). Complex **5a** (as BF_4^- salt, **5a**BF_4) was already prepared by an alternative method recently.[16] It has to be noted that an analogous complex [Fe(PNP^{CH2}-Ph)]$_2^{2+}$ bearing CH_2-spacers between the pyridine ring and the PPh_2 moieties was reported.[23] In the case of [Fe(κ^3-*P,N,P*-PNP-BIPOL)(κ^2-*P,N*-PNP-BIPOL)Cl]$^+$ (**2b**) rapid decomposition took place in all common solvents such as CH_2Cl_2, CH_3CN, or THF also in the absence of halide scavengers such as $AgCF_3SO_3$. However, fortunately from this mixture in THF as solvent small amounts of crystals of **5b**CF_3SO_3 suitable for an X-ray diffraction study could be obtained by slow solvent evaporation. Other decomposition products could not be identified. Complex [Fe(κ^3-*P,N,P*-PNP-Me)(κ^2-*P,N*-PNP-Me)Cl]$^+$ (**2c**) is unstable in solution and readily forms the dicationic complex [Fe(κ^3-*P,N,P*-PNP-Me)$_2$]$^{2+}$ (**5c**) even in the absence of halide scavengers. Perhaps unexpected, in contrast to **2c** the Et, *n*Pr, and *n*Bu-analog complexes [Fe(κ^3-*P,N,P*-PNP-Et)(κ^2-*P,N*-PNP-Et)Cl]$^+$ (**2e**), [Fe(κ^3-*P,N,P*-PNP-*n*Pr)(κ^2-*P,N*-PNP-*n*Pr)Cl]$^+$ (**2g**), and [Fe(κ^3-*P,N,P*-PNP-*n*Bu)(κ^2-*P,N*-PNP-*n*Bu)Cl]$^+$ (**2h**), respectively, are stable in solution for several days without any noticeable rearrangement reactions. In the presence of halide scavengers, however, the dicationic complexes [Fe(κ^3-*P,N,P*-PNP-Et)$_2$]$^{2+}$ (**5d**), [Fe(κ^3-*P,N,P*-PNP-*n*Pr)$_2$]$^{2+}$ (**5e**) and [Fe(κ^3-*P,N,P*-PNP-*n*Bu)$_2$]$^{2+}$ (**5f**) are readily formed. Since the electron donating properties of these PNP ligands are very similar, the observed reactivity differences may be due to steric reasons. Cone angles determined from crystallographic data reveal that PNP-Me is the sterically least demanding ligand in this series.

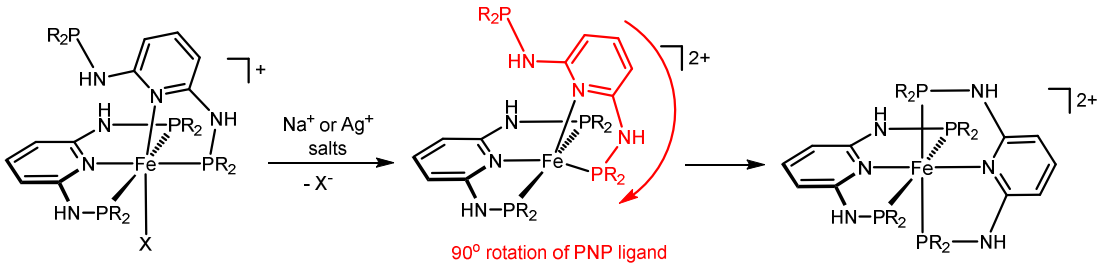

Scheme 5

With the exception of **5b**, all complexes of the type $[Fe(\kappa^3\text{-}P,N,P\text{-PNP})_2]^{2+}$ were characterized by ^1H and $^{31}P\{^1H\}$ NMR spectroscopy, and elemental analysis. In the case of complexes **5c-f** also $^{13}C\{^1H\}$ NMR spectra were recorded. Complexes **5a** and **5c-f** exhibit a singlet resonance in the $^{31}P\{^1H\}$ NMR spectrum at 98.2, 108.3, 119.0, 114.2, and 115.0 ppm, respectively. In the ^1H NMR spectrum the NH protons give rise to a slightly broadened singlet in the range 7 to 8 ppm. All other resonances are unremarkable and are not discussed here.

ESI-MS enables the detection and the study of reaction substrates and products but also of short-lived reaction intermediates and decomposition products as they are present in solution. Accordingly, solutions of $[Fe(\kappa^3\text{-}P,N,P\text{-PNP-Ph})(\kappa^2\text{-}P,N\text{-PNP-Ph})Cl]Cl$ (**2a**Cl) and $[Fe(\kappa^3\text{-}P,N,P\text{-PNP-Et})(\kappa^2\text{-}P,N\text{-PNP-Et})Cl]Cl$ (**2e**Cl) in CH_3OH were subjected to ESI-MS analysis in the positive ion mode. The most abundant signal observed corresponds to the intact complexes **2a** and **2e** ($[M]^+$) at *m/z* 1045.4 and 661.2, respectively, emphasizing the relative stability of this complex. Further, small signals were found at *m/z* 505.2 and 313.1, respectively, assignable to the doubly charged complexes $[Fe(\kappa^3\text{-}P,N,P\text{-PNP-Ph})_2]^+$ (**5a**) and $[Fe(\kappa^3\text{-}P,N,P\text{-PNP-Et})_2]^+$ (**5e**), $[M\text{-Cl}]^{2+}$, where the chloride ligand is dissociated. Moreover, weak signals were detected at *m/z* is 568.2 and 376.1, respectively, due to loss of a PNP ligand, $[M\text{-PNP}]^+$. The ESI full scan mass spectrum of **2eCl** in CH_3OH is depicted in Figure 7. The fragmentation of the selected **2a** and **2e** ions $[M]^+$ with *m/z* 1045.4 and 661.2 by low energy collision-induced dissociation (CID) in an ion trap analyzer resulted in the formation of ions with *m/z* 568.2 and 376.1, respectively, due to loss of one PNP ligand ($[M\text{-PNP}]^+$). The results of the ESI MS studies again support that both the halide and the κ^2-*P,N*-bound PNP ligands are substitutionally labile.

Figure 7

Structural views of the $[Fe(\kappa^3\text{-}P,N,P\text{-PNP})_2]$ complexes **5a**Cl, **5b**CF_3SO_3, **5c**CF_3SO_3, **5d**BPh_4, and **5e**BF_4 are depicted in Figures 8 - 12 with selected bond distances given in the caption. The five complexes show modestly distorted and relatively uniform octahedral coordination figures about Fe, each coordinated by two N in axial and four P in equatorial disposition. The Fe-N bond distances vary

between 1.956 and 2.032 Å, mean value 1.995 Å, and the N-Fe-N bond angles are nearly straight, varying between 178.23 and 180°. The Fe-P bond lengths are short for the complex **5b**CF_3SO_3 with the phosphite ligands (mean value Fe-P 2.183 Å), intermediate for the PPh_2-based ligand in **5a**Cl (Fe-P 2.252 Å), and longest for the P(alkyl)$_2$-based ligands of complexes **5c**CF_3SO_3, **5d**BPh_4, and **5e**BF_4 (mean values Fe-P 2.275, 2.292, and 2.274 Å for PMe_2 in **5c**CF_3SO_3, PEt_2 in **5d**BPh_4, and P*n*Pr_2 in **5e**BF_4). The *trans*-bond angles P-Fe-P deviate notable from 180° by varying between 154.92 (**5e**BF_4) to 168.93° (**5a**Cl). Despite the relatively uniform FeN_2P_4 octahedra, there are significant differences between the complexes with respect to the planarity the chelate rings Fe-P-N-C-N-(Fe) and related with this whether the two pyridine rings of each complex are oriented mutually perpendicular or whether they are less inclined to each other. The first case with mutually perpendicular pyridine rings is represented by the PPh_2-based complex **5a**Cl. In it the phenyl rings of adjacent PPh_2 groups are most relaxed when they are in pair-wise stabilizing π-π contacts (*cf* Figure 8). The ideal point symmetry of such a complex would be -42m (D_{2d}) from which complex **5a**Cl deviates only a little and has point symmetry -4 (S_4) instead. Like in complex **5a**Cl the chelate rings in complex **5b**CF_3SO_3 are essentially flat and the two pyridine rings subtend an interplanar angle of 88.6°. Due to the steric features of the bipol ligand the complex in **5b**CF_3SO_3 adopts approximately the symmetry 222 (D_2). In the P(alkyl)$_2$-based complexes **5c**CF_3SO_3, **5d**BPh_4, and **5e**BF_4 the chelate rings about Fe are distinctly non-planar and the two pyridine rings mutually inclined at angles of 57.78° (**5c**CF_3SO), 41.56° (**5d**BPh_4), and 34.61° (**5e**BF_4), which decrease with increasing alkyl chain length (**5c**CF_3SO_3: Me; **5d**BPh: Et, **5e**BF_4: *n*-Pr). In the same order the P-Fe-P *trans*-angles diminish from 163.38° *via* 157.17° to 154.92°. These changes, pyridine interplanar angle and P-Fe-P *trans*-angles, are considered to be largely due to the increased steric demand of the alkyl substituents of phosphorus.

Figures 9 - 13

The pendant arm of complexes **2** may be readily oxidized to the respective phosphine oxides and sulfides in the presence of hydrogen peroxide and elemental sulfur. This was exemplarily examined for **2g**. While oxidation with hydrogen peroxide led to several not identified decomposition products, the reaction with 1 equiv of sulfur afforded cleanly [Fe(κ^3-*P,N,P*-PNP-*n*Pr)(κ^2-*P,N*-PNS-*n*Pr)Cl]$^+$ (**6**) in 91% isolated yield (Scheme 6). This complex features a new κ^2-P,N-bound SNP ligand as apparent from the $^{31}P\{^1H\}$ NMR spectrum. Oxidation of the phosphorous atom of the pendant P*n*Pr_2-NH-arm to give a S=P*n*Pr_2-NH-moiety is accompanied by a high field shift from 27.5 to 64.6 ppm. The phosphorus atoms of the coordinated κ^3-PNP and κ^2-SNP ligands again give raise to a characteristic A_2B pattern (Figure 1). Interestingly, treatment of **6** with 1 equiv of $AgBF_4$ did not result in coordination of the phosphine sulfide moiety to give [Fe(κ^3-*P,N,P*-PNP-*n*Pr)(κ^3-*S,P,N*-PNS-*n*Pr)Cl]$^+$ but led to liberation of the SNP ligand and formation of the known homoleptic dicationic complex **5e** (Scheme 6).

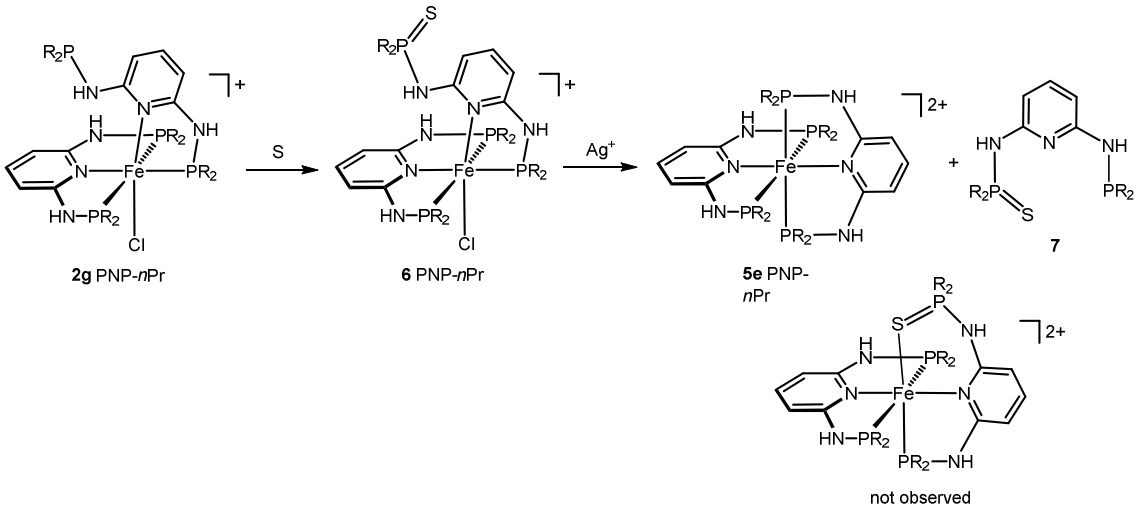

Scheme 6

Conclusion

In the present paper, we investigated the reaction of iron(II) halides with a series of PNP pincer ligands based on the 2,6-diaminopyridine scaffold. The steric bulk of PNP ligands prepared thus far decrease in the order PNP-*t*Bu (130) > PNP^{Me}-*i*Pr (120) ≈ PNP^{Ph}-*n*Pr ≈ PNP^{Ph}-Et (120) > PNP-*i*Pr (115) > PNP^{Me}-Ph (105)> PNP-*n*Bu ≈ PNP-*n*Pr ≈ PNP-Et ≈ PNP-Ph (100) > PNP-BIPOL (95) > PNP-Me (90). With PNP ligands which are sterically less demanding than PNP-*i*Pr complexes of the type [Fe(κ^3-*P,N,P*-PNP)(κ^2-*P,N*-PNP)X]$^+$ (X = Cl, Br) were formed, while with the bulkier ligands pentacoordinate complexes [Fe(κ^3-*P,N,P*-PNP)X_2] were obtained. In the case of the first, the PNP pincer ligands are coordinated in κ^3-*P,N,P*- and κ^2-*P,N*-fashion, respectively, and adopt a strongly distorted octahedral geometry as established by X-ray crystallography. Obviously related to these distortions is their reactivity undergoing, upon halide dissociation, a facile rearrangement reaction to give the dicationic complexes [Fe(κ^3-*P,N,P*-PNP)$_2$]$^{2+}$ where now both PNP ligands are bound in κ^3-*P,N,P*-fashion. This reaction proceeds only in the case of the smaller PNP ligands (PNP-Ph, PNP-BIPOL, PNP-Me), while with the bulkier ones (PNP-*n*Bu, PNP-*n*Pr, PNP-Et) the presence of a halide scavenger is required. The outcome of these investigation strongly suggests that the formation and reactivity of [Fe(κ^3-*P,N,P*-PNP)(κ^2-*P,N*-PNP)X]$^+$ complexes is controlled by the steric bulk of the PNP ligands rather than their electronic properties.

Experimental Section

General. All manipulations were performed under an inert atmosphere of argon by using Schlenk techniques or in an MBraun inert-gas glovebox. The solvents were purified according to standard procedures.[24] The deuterated solvents were purchased from Aldrich and dried over 4 Å molecular sieves. The ligands N,N'-bis(dibenzo[d,f][1,3,2]dioxaphosphepine)-2,6-diaminopyridine (PNP-BIPOL) (**1b**)[17] and N,N'-bis(diphenylphosphino)-N,N'-dimethyl-2,6-diaminopyridine (PNP^{Me}-Ph)[16] (**1g**), and

[Fe(κ^3-*P,N,P*-PNP-Ph)(κ^2-*P,N*-PNP-Ph)Cl]Cl (**2a**Cl)[15] were prepared according to the literature. ^{1}H, ^{13}C{^{1}H}, and ^{31}P{^{1}H} NMR spectra were recorded on Bruker AVANCE-250, AVANCE-300 DPX, and AVANCE-400 spectrometers. ^{1}H and ^{13}C{^{1}H} NMR spectra were referenced internally to residual protio-solvent, and solvent resonances, respectively, and are reported relative to tetramethylsilane (δ = 0 ppm). ^{31}P{^{1}H} NMR spectra were referenced externally to H_3PO_4 (85%) (δ = 0 ppm). Room-temperature solution (CH_2Cl_2) magnetic moments were determined by ^{1}H NMR spectroscopy using the method of Evans.[25]

All mass spectrometric measurements were performed on an Esquire 3000^{plus} 3D-quadrupole ion trap mass spectrometer (Bruker Daltonics, Bremen, Germany) in positive-ion mode by means of electrospray ionization (ESI). Mass calibration was done with a commercial mixture of perfluorinated trialkyl-triazines (ES Tuning Mix, Agilent Technologies, Santa Clara, CA, USA). All analytes were dissolved in methanol "hypergrade for LC-MS Lichrosolv" quality (Merck, Darmstadt, Germany) to form a concentration of roughly 1 mg/mL. Direct infusion experiments were carried out using a Cole Parmer model 74900 syringe pump (Cole Parmer Instruments, Vernon Hills, IL, USA) at a flow rate of 2 μL/min. Full scan and MS/MS (low energy CID)-scans were measured in the range m/z 100-1100 with the target mass set to m/z 1000. Further experimental conditions include: drying gas temperature: 150°C; capillary voltage: -4 kV; skimmer voltage: 40 V; octapole and lens voltages: according to the target mass set. Helium was used as buffer gas for full scans and as collision gas for MS/MS-scans in the low energy CID mode. The activation and fragmentation width for tandem mass spectrometric (MS/MS, CID) experiments was set to 6 Da to cover the main isotope cluster for fragmentation. The corresponding fragmentation amplitude ranged from 0.4 to 0.6 V in order to keep a precursor ion intensity of low abundance in the resulting MS/MS spectrum. All mass calculations are based on the lowest mass (i.e. most abundant) iron isotope (^{56}Fe-isotope). Mass spectra and CID spectra were averaged during data acquisition time of 1 to 2 min and one analytical scan consisted of five successive micro scans resulting in 50 and 100 analytical scans, respectively, for the final full scan mass spectrum or MS/MS spectrum.

N,N'-Bis(dimethylphosphino)-2,6-diaminopyridine (PNP-Me) (1c). A suspension of 2,6-diaminopyridine (500 mg , 4.6 mmol) in THF (20 mL) was cooled to 0°C and NEt_3 (1.3 mL, 9.2 mmol) was added. Then a solution of Me_2PCl (0.88g, 9.90 mmol) in THF (10 mL) was added slowly via a dropping-funnel. The mixture was then allowed to reach room temperature and stirred for 12 h. The mixture was filtrated over Celite and washed with THF (5 mL). After removal of the solvent under reduced pressure, a pale red oil was obtained which afforded white crystals in the freezer at -20°C. Yield: 0.93 g (89 %). Anal. Calcd. for $C_9H_{17}N_3P_2$ (229.20). C, 47.16; H, 7.48; N, 18.33. Found: C, 46.98; H, 7.81; N, 18.27.^{1}H NMR (δ, $CDCl_3$, 20°C): 7.25 (t, J_{HH} = 8.5 Hz, 1H, py^4), 6.25 (d, J_{HH} = 8.3 Hz, 2H, py^{3,5}), 4.35 (s, broad, 2H, NH), 1.26 (d, J_{HP} = 4.5 Hz, 2H, C*H*$_3$). ^{13}C{^{1}H} NMR (δ, $CDCl_3$, 20°C): 157.4 (py), 139.5 (d, J_{CP} = 16.3 Hz, py), 97.8 (py), 6.1 (d, J_{CP} = 8.0 Hz, *C*H$_3$). ^{31}P{^{1}H} NMR (δ, $CDCl_3$, 20°C): 14.1.

N,N'-Bis(diethylphosphino)-2,6-diaminopyridine (PNP-Et) (1d). A suspension of 2,6-diaminopyridine (590 mg , 5.4 mmol) in toluene (15 mL) was cooled to 0°C and NEt_3 (1.5 mL, 10.8 mmol) was added. Then a solution of Et_2PCl (1.34 g, 10.8 mmol) in toluene (10 mL) was added slowly

via a dropping-funnel. The mixture was then allowed to reach room temperature and stirred for 12 h. The mixture was filtrated over Celite and washed with toluene (5 mL). After removal of the solvent under reduced pressure, a pale red oil was obtained which afforded white crystals in the freezer at -20°C. Yield: 1.46 g (96 %). Anal. Calcd. for $C_{13}H_{25}N_3P_2$ (285.31): C, 54.73; H, 8.83; N, 14.73. Found: C, 54.53; H, 8.91; N, 14.70. ^{1}H NMR (δ, $CDCl_3$, 20°C): 7.25 (t, J_{HP} = 8.4 Hz, 1H, py^4), 6.37 (d, J_{HP} = 8.1 Hz, 2H, py^{3,5}), 4.26 (d, J_{HP} = 9.3 Hz, 2H, NH) 1.55 (dq, J_{HH} = 7.4 Hz, J_{HP} = 14.3 Hz, 8H, C*H*$_2$), 1.05 (dt, J_{HH} = 7.6 Hz, J_{HP} = 15.3 Hz, 12H, C*H*$_3$). ^{13}C{^{1}H} NMR (δ, $CDCl_3$, 20°C): 158.7 (d, J_{CP} = 18.1 Hz, py), 139.2 (s, py), 98.1 (d, J_{CP} = 17.7 Hz, py), 23.6 (d, J_{CP} = 11.9 Hz, *C*H$_2$), 8.5 (d, J_{CP} = 13.0 Hz, *C*H$_3$). ^{31}P{^{1}H} NMR (δ, $CDCl_3$, 20°C): 33.2.

N,N'-Bis(ethylphosphino)-N,N'-diphenyl-2,6-diaminopyridine (PNP^{Ph}-Et) (1h). 1h was prepared analogously to **1d** with N,N'-diphenyl-2,6-diaminopyridine (500 mg, 1.9 mmol) and Et_2PCl (480 mg, 3.8 mmol) as starting materials. After workup the product is obtained as a white solid. Yield: 770 mg (90 %). Anal. Calcd. for $C_{25}H_{33}N_3P_2$ (437.50): C, 68.63; H, 7.60; N, 9.60. Found: C, 68.33; H, 7.87; N, 9.50. ^{1}H NMR (δ, $CDCl_3$, 20°C): 7.38 (m, 4H, Ph), 7.22 (t, J_{HH} = 7.2 Hz, 1H, py^4), 7.08 (m, 6H, Ph), 5.99 (d, J_{HH} = 8.0 Hz, 2H, py^{3,5}), 1.78 (m, 4H, CH_2), 1.28 (m, 4H, CH_2), 1.04 (m, 12H, CH_3). ^{13}C{^{1}H} NMR (δ, $CDCl_3$, 20°C): 160.2 (d, J_{CP} = 11.9 Hz, py), 137.7 (py), 130.1 (Ph), 130.0 (Ph), 129.2 (Ph), 125.9 (Ph), 102.0 (d, J_{CP} = 8.9 Hz, py), 21.3 (d, J_{CP} = 13.8 Hz, *C*H$_2$), 9.6 (d, J_{CP} = 18.3 Hz, *C*H$_3$). ^{31}P{^{1}H} NMR (δ, $CDCl_3$, 20°C): 57.1.

N,N'-Bis(*n*-propylphosphino)-N,N'-diphenyl-2,6-diaminopyridine (PNP^{Ph}-*n*Pr) (1i). 1i was prepared analogously to **1d** with N,N'-diphenyl-2,6-diaminopyridine (500 mg, 1.9 mmol) and Et_2PCl (580 mg, 3.8 mmol) as starting materials. After workup the product is obtained as a pale-yellow solid. Yield: 860 mg (92 %). Anal. Calcd. for $C_{29}H_{41}N_3P_2$ (493.60): C, 70.56; H, 8.37; N, 8.51. Found: C, 70.34; H, 8.44; N, 8.69. ^{1}H NMR (δ, $CDCl_3$, 20°C): 7.34 (m, 4H, Ph), 7.20 (m, 1H, py^4), 7.05 (d, J_{HH} = 7.6 Hz, 6H, Ph), 5.98 (d, J_{HH} = 7.9 Hz, 2H, py^{3,5}), 1.86 (m, 4H, CH_2), 1.50-1.39 (m, 8H, CH_2), 1.25-1.17 (m, 4H, CH_2), 0.95 (dt, J_{HH} = 7.1 Hz, J_{HP} = 2.5 Hz, 12H, CH_3). ^{13}C{^{1}H} NMR (δ, $CDCl_3$, 20°C): 160.3 (d, J_{CP} = 10.4 Hz, py), 144.4 (Ph), 137.6 (py), 130.1 (Ph), 129.2 (Ph), 125.7 (Ph), 102.0 (d, J_{CP} = 9.1 Hz, py), 31.3 (d, J_{CP} = 15.6 Hz, *C*H$_2$), 19.0 (d, J_{CP} = 18.3 Hz, *C*H$_2$) 15.8 (d, J_{CP} = 13.3 Hz, *C*H$_3$). ^{31}P{^{1}H} NMR (δ, $CDCl_3$, 20°C): 49.6.

[Fe(κ^3-*P,N,P*-PNP-BIPOL)(κ^2-*P,N*-PNP-BIPOL)Cl]Cl (2bCl**).** To a suspension of anhydrous $FeCl_2$ (58 mg, 0.46 mmol) in THF (15 mL) PNP-BIPOL (**1b**) (500 mg, 0.93 mmol) was added and the mixture was stirred for 4 h. The resulting green solution was evaporated to dryness and the remaining green solid was washed with diethyl ether (30 mL) and dried under vacuum. Yield: 422 mg (90 %). Anal. Calcd. for $C_{58}H_{42}Cl_2FeN_6O_8P_4$ (1201.64): C, 57.97; H, 3.52; N, 6.99. Found: C, 57.77; H, 3.49; N, 7.11. ^{1}H NMR (δ, CD_2Cl_2, 20°C): 7.66-7.00 (m, 31 H), 6.85 (d, J_{HH} = 7.5 Hz, 4H, py), 6.56 (d, J_{HP} = 7.5 Hz, 3H, NH), 6.40 (t, 2H, py), 6.13 (d, J_{HP} = 7.5 Hz, 1H, NH). ^{31}P{^{1}H} NMR (δ, CD_2Cl_2, 20°C): A_2B spin system, δ_A = 192.4 (2P), δ_B = 182.1 (1P), J_{PP} = 110 Hz (shifts and J_{PP} determined from simulation), 146.2 (1P).

[Fe(κ^3-*P,N,P*-PNP-Me)(κ^2-*P,N*-PNP-Me)Cl]Cl (2cCl**).** A solution of PNP-Me (**1c**) (100 mg, 0.44 mmol) in acetone (8 mL) was reacted with anhydrous $FeCl_2$ (27 mg, 0.22 mmol) and was stirred

for 6 h, whereupon a green precipitate was formed. The solid was filtrated and washed with acetone (5 mL), diethyl ether (5 mL), and dried under vacuum. Yield: 120 mg (95%). Anal. Calcd. for $C_{18}H_{34}Cl_2FeN_6P_4$ (585.15): C, 36.95; H, 5.86; N, 14.36. Found: C, 36.67; H, 5.97; N, 14.40.

[Fe(κ^3-*P,N,P*-PNP-Me)(κ^2-*P,N*-PNP-Me)Br]Br (2dBr**).** This compound was prepared analogously to **2e** using **1c** (100 mg, 0.44 mmol) and anhydrous $FeBr_2$ (46 mg, 0.22 mmol) as starting materials. Yield: 139 mg (95%). Anal. Calcd. for $C_{18}H_{34}Br_2FeN_6P_4$ (674.05): C, 32.07; H, 5.08; N, 12.47. Found: C, 32.24; H, 4.94; N, 11.81.

[Fe(κ^3-*P,N,P*-PNP-Et)(κ^2-*P,N*-PNP-Et)Cl]BPh$^{Me}_4$ (2eBPh^{Me}_4**).** A solution of PNP-Et (**1d**) (200 mg, 0.70 mmol) and $FeCl_2$ (44 mg, 0.35 mmol) in THF (10 mL) was stirred for 1 h at room temperature. A green precipitate was formed which was collected on a glass frit, washed with THF (5mL) and dried under vacuum. Yield: 232 mg (95%) of [Fe(κ^3-*P,N,P*-PNP-Et)(κ^2-*P,N*-PNP-Et)Cl]Cl. Anal. Calcd. for $C_{26}H_{50}Cl_2FeN_6P_4$ (697.36): C, 44.78; H, 7.23; N, 12.05. Found: C, 44.23; H, 6.94; N, 12.06. In order to obtain a soluble complex, this compound was suspended in 8 mL of THF and $NaBPh^{Me}_4$ was added (139 mg, 0.35 mmol). After stirring for 30 min the solution was evaporated to dryness and the residue was resolved in CH_2Cl_2 (10 mL) and filtrated over Celite. The solvent was then removed under reduced pressure and the green solid was washed with *n*-hexane (10 mL) and dried under vacuum. Crystals of **2e**BPh^{Me}_4 were grown from a THF solution by slow diffusion of diethyl ether. Yield 323 mg (89%). Anal. Calcd. for $C_{54}H_{78}BClFeN_6P_4 \cdot C_{12}H_{24}O_3$ (1253.58): C, 63.24; H, 8.20; N, 6.70. Found: C, 62.98; H, 8.94; N, 6.56. ^{1}H NMR (δ, CD_2Cl_2, 20°C): 8.21 (s, 2H, NH), 7.92 (s, 1H, NH), 7.54 (t, J_{HP} = 8.1 Hz, 1H, py), 7.30 (m, 8H, Ph), 7.06 (t, J_{HP} = 7.8 Hz, 1H, py), 6.79 (m, 8H, Ph), 6.64 (d, J_{HP} = 8.0 Hz, 2H, py), 6.36 (dd, J_{HP} = 4.8 Hz, 1H, py), 6.07 (d, J_{HP} = 7.7 Hz, 1H, py), 4.91 (d, J_{HP} = 9.5 Hz, 1H, NH), 2.85-2.54 (m, 8H, C*H*$_2$), 2.51-2.34 (m, 4H, C*H*$_2$), 2.15 (s, 12H, C*H*$_3$), 2.07-2.00 (m, 18H, C*H*$_3$), 1.38-1.31 (m, C*H*$_2$), 1.10-0.85 (m, C*H*$_3$). ^{31}P{^{1}H} NMR (δ, CD_2Cl_2, 20°C): A_2B spin system, δ_A = 114.4 (2P), δ_B = 111.4 (1P), J_{PP} = 50 Hz (shifts and J_{PP} determined from simulation), 36.3 (1P).

[Fe(κ^3-*P,N,P*-PNP^{Me}-Ph)(κ^2-*P,N*-PN^{NHMe}-Ph)Cl]BF_4 (3). To a suspension of anhydrous $FeCl_2$ (127 mg, 1.0 mmol) in THF (10 mL) PNP^{Me}-Ph (**1g**) (1.02 g, 2.00 mmol) and $AgBF_4$ (195 mg, 1.0 mmol) was added and the mixture was stirred for 4h. The solvent was removed under reduced pressure and the remaining green solid was dissolved in CH_2Cl_2. The white precipitate (AgCl) was removed by filtration over Celite and the solution was evaporated under reduced pressure. The remaining green solid was washed twice with diethyl ether (10 mL) and dried under vacuum. Yield: 950 mg (94%). Crystals of **3** were grown by slow diffusion of diethyl ether into a solution of THF. Anal. Calcd. for $C_{50}H_{49}BClF_4FeN_6P_3$ (1005.00): C, 59.76; H, 4.91; N, 8.36. Found: C, 59.83; H, 4.86; N, 8.31. ^{1}H NMR (δ, CD_2Cl_2, 20°C): 6.80-8.10 (m, 41H, py, Ph), 2.97 (bs, 9H, C*H*$_3$). ^{31}P{^{1}H} (δ, CD_2Cl_2, 20°C): A_2B spin system, δ_A = 128.1 (2P), δ_B = 122.6 (1P), J_{PP} = 46 Hz (shifts and J_{PP} determined from simulation).

[Fe(κ^3-*P,N,P*-PNP^{Ph}-Et)(Cl)$_2$] (4a). A suspension of **1h** (100 mg, 0.23 mmol) and anhydrous $FeCl_2$ (29 mg, 0.23 mmol) in THF (7 mL) was stirred for 1h. After that the solvent was removed under reduced pressure and a yellow solid was obtained which washed with 10 mL of *n*-hexane and dried

under vacuum. Yield: 125 mg (97%). Anal. Calcd. for $C_{25}H_{33}Cl_2FeN_3P_2$ (564.25): C, 53.22; H, 5.89; N, 7.45. Found: C, 53.33; H, 5.83; N, 7.71. μ_{eff} = 4.9 μ_B.

[Fe(κ^3-*P,N,P*-PNP^{Ph}-*n*Pr)(Cl)$_2$] (4b). This complex was prepared analogously to **4a** using PNP^{Ph}-*n*Pr (**1i**) (150 mg, 0.30 mmol) in THF (7 mL) and anhydrous $FeCl_2$ (38 mg, 0.30 mmol) as reactants. Yield: 180 mg (95%). Anal. Calcd. for $C_{29}H_{41}Cl_2FeN_3P_2$ (620.35): C, 56.15; H, 6.66; N, 6.77. Found: C, 56.00; H, 6.53; N, 6.87. μ_{eff} = 4.8 μ_B.

[Fe(κ^3-*P,N,P*-PNP-Ph)$_2$](Cl)$_2$ (5aCl**).** A solution of complex **2a**Cl (50mg) in 5 mL of CH_3CN was stirred for 15 min, whereupon the color changed from green to red. The solvent was evaporated and the remaining red solid was washed with diethyl ether and dried in vacuum. Yield: 45 mg (90 %yield). All spectral data for **5a**Cl were identical with those of the authentic sample **5a**BF_4 reported previously.[16] Crystals for X-ray diffraction were obtained by slow solvent evaporation from a mixture of methanol and diethyl ether.

[Fe(κ^3-*P,N,P*-PNP-BIPOL)$_2$](CF$_3$SO$_3$)$_2$ (5bCF_3SO_3**).** Small amounts of crystals of **5b**CF_3SO_3 suitable for X-ray crystallography could be obtained by reacting **2b**Cl in THF with two equivs of $AgCF_3SO_3$ followed by solvent evaporation. However, this complex could not be isolated in pure form and crystals were taken from a mixture of several intractable solid products.

[Fe(κ^3-*P,N,P*-PNP-Me)$_2$](BF$_4$)$_2$ (5cBF_4**).** A solution of **1c** (100 mg, 0.44 mmol) and anhydrous $FeCl_2$ (27 mg, 0.22 mmol) in acetone (10 mL) was stirred for 1 h. After that $AgBF_4$ (86 mg, 0.44 mmol) was added and the mixture was stirred for an additional hour, whereupon the color of the solution changed from green to purple. The solution was filtrated over Celite, and the solvent was removed under reduced pressure. The purple solid was washed with 15 mL of *n*-hexane and was then dried under vacuum. Yield: 144 mg (95%). Anal. Calcd. for $C_{18}H_{34}FeFeN_6P_4B_2F_8$ (687.85): C, 31.43; H, 4.98; N, 12.22. Found: C, 30.79; H, 4.80; N, 11.98. ^{1}H NMR (δ, acetone-d_6, 20°C):7.48 (s, 4H, NH), 7.22 (t, J_{HH} = 9.5 Hz, 2H, py), 6.17 (d, J_{HH} = 9.5 Hz, 4H, py), 2.10 (s, 24H, C*H*$_3$). ^{13}C{^{1}H} NMR (δ, acetone-d_6, 20°C): 162.4 (py), 140.0 (py), 100.3 (py), 23.3 (t, J_{CP} = 18 Hz, *C*H$_3$). ^{31}P{^{1}H} NMR (δ, acetone-d_6, 20°C): 108.3. Crystals suitable for X-ray crystallography were grown with $CF_3SO_3^-$ as counterion (analogously prepared with $AgCF_3SO_3$ as halide scavenger) from an acetone solution by slow diffusion of diethyl ether.

[Fe(κ^3-*P,N,P*-PNP-*n*Pr)(κ^2-*P,N*-PNS-*n*Pr)Cl]BF$_4$ (6). To a solution of PNP-*n*Pr (**1e**) (200 mg, 0.59 mmol) in acetone (7 mL) anhydrous $FeCl_2$ (37 mg, 0.29 mmol) and $NaBF_4$ (28 mg, 0.25 mmol) was added and the mixture was stirred for 1 h. Elemental sulfur (8.0 mg, 0.25 mmol) was then added and the solution was stirred for additional 2 h. The green suspension was then filtrated over Celite and the solution was evaporated to dryness. The remaining solid was washed with diethyl ether (5 mL) and *n*-hexane (10 mL). The remaining green powder was dried in vacuum. Yield: 204 mg (91 %). Anal. Calcd. for $C_{34}H_{66}BClF_4FeN_6P_4S$ (892.99): C, 45.73; H, 7.45; N, 9.42. Found: C, 45.81; H, 7.39; N, 9.36. ^{1}H NMR (δ, acetone-d_6, 20°C): 8.14 (s, 2H, NH), 7.89 (s, 1H, NH), 7.48 (m, 1H, py^4), 7.22 (m, 1H, py^4), 6.64 (m, 2H, py^{3,5}), 6.33 (m, 1H, py^3), 5.88 (d, J_{HH} = 7.8 Hz, py^5), 4.96 (s, 1H, NH), 2.70-2.18 (m, 4H, CH_2), 1.88-1-39 (m, 4H, CH_2), 1.10-0.90 (m, 15H, CH_2, CH_3), 0.64 (m, 3H, CH_3). ^{13}C{^{1}H} NMR (δ, acetone-d_6, 20°C): 164.6 (m, py), 164.3-164.5 (m, py), 140.8 (py), 138.0 (py), 101.3 (py), 100.7 (py),

100.1 (py), 37.4 (m, CH_2), 34.0 (CH_2), 32.9 (CH_2), 30.8 (d, J_{CP} = 10.8 Hz, *C*H_2), 17.1-14.3 (*C*H_2, *C*H_3). $^{31}P\{^1H\}$ NMR (δ, acetone-d_6, 20°C): A_2B spin-system, δ_A = 109.4 (2P), δ_B = 108.6 (1P), J_{PP} = 50 Hz (shifts and J_{PP} determined from simulation), 64.6 (1P).

X-ray Structure Determination. X-ray diffraction data were collected at *T* = 100 K in a dry stream of nitrogen on Bruker Kappa APEX II (complexes **2e**BPh^{Me}_4, **2f**BPh^{Me}_4, **3**, **5a**Cl, **5b**CF_3SO_3, **5c**CF_3SO_3, **5d**BPh_4, and **5e**BF_4) diffractometer systems using graphite-monochromatized Mo-*K*α radiation (λ = 0.71073 Å) and fine sliced *φ*- and *ω*-scans. Data were reduced with the program SAINT-Plus[26] and corrections for absorption and detector effects were applied with the program SADABS.[25] The structures of complexes **2f**BPh^{Me}_4, **5a**Cl, **5b**CF_3SO_3, and **5d**BPh_4 were solved with direct methods and refined with the SHELXTL program package.[27] The structures of complexes **2e**BPh^{Me}_4, **3**, **5c**CF_3SO_3, and **5e**BF_4 were solved with charge-flipping implemented in SUPERFLIP[28] and refined using Jana2006.[29] All refinements were against F^2 data. Non-hydrogen atoms were refined anisotropically. The H atoms connected to C atoms were placed in calculated positions and thereafter refined as riding on the parent atoms. H atoms connected to N atoms were mostly located in difference Fourier maps and freely refined. Molecular graphics were generated with the program MERCURY.[30] Crystal data and experimental details are given in the ESI (Table S1 and CIF).

Variata: Seven of the eight crystal structures concerned solvates, namely: **2e**BPh^{Me}_4·3THF, **2f**BPh^{Me}_4·3THF, **5a**Cl·solv (solv = CH_3OH, Et_2O), **5b**CF_3SO_3·6.5THF, **5c**CF_3SO_3·$2Me_2CO$, **5d**BPh_4·$0.5Et_2O$, and **5e**BF_4·$2Me_2CO$. Only compound **3** was an unsolvated tetrafluoroborate salt. Complex **2e**BPh^{Me}_4·3THF and **2f**BPh^{Me}_4·3THF, a chloride and a bromide complex, represent an isostructural pair. A small peak in the difference Fourier map of **2e**BPh^{Me}_4·3THF was attributed to a partially oxidized uncoordinated phosphine P atom. The site was therefore refined as a partially occupied isotropic O atom, whereby the occupancy refined to 0.162(7). Complex **5a**Cl·solv: The solvent in this solid, a mixture of methanol and diethyl ether, was disordered and was therefore removed from the structure factors with procedure SQUEEZE of program PLATON[31] prior to concluding refinement. Complex **5b**CF_3SO_3·6.5THF: This was a weakly scattering solvent-rich material with 6.5 THF molecules per formula unit. One THF was disordered about a centre of symmetry and one of two CF_3SO_3 groups was orientation disordered. This highly desolvation-prone material scattered only to θ ca. 25° and gave somewhat meagre R values for a lastly very reasonable crystal structure. Complex **5c**CF_3SO_3·$2Me_2CO$: In this crystal structure the Fe complex **5c**CF_3SO_3·$2Me_2CO$ and one acetone molecule are located on 2-fold axes (point symmetry C_2) while another acetone molecule is disordered about an inversion. Complex **5d**BPh_4·$0.5Et_2O$: In this crystal structure the diethyl ether molecule is disordered about an inversion. **5e**BPh_4·$2Me_2CO$: In this crystal structure the Fe complex has point symmetry 222 (D_2) and the ordered acetone molecule point symmetry 2 (C_2).

Computational Details. All calculations were performed using the GAUSSIAN 09 software package[32] on the Phoenix Linux Cluster of the Vienna University of Technology. The optimized geometries were obtained with the B3LYP functional,[33] without symmetry constraints. That functional includes a mixture of Hartree-Fock[34] exchange with DFT[35] exchange-correlation, given by Becke's three parameter functional with the Lee, Yang and Parr correlation functional, which includes both

local and non-local terms. The basis set used for the geometry optimizations consisted of the Stuttgart/Dresden ECP (SDD) basis set[36] to describe the electrons of iron, and a standard 6-31g** basis set[37] for all other atoms. A Natural Population Analysis (NPA)[38] and the resulting Wiberg indices[21] were used to study the electronic structure and bonding of the optimized species.

The inclusion of dispersion effects by means of Grimme DFT-D3 method[39] with Becke and Jonhson short distance damping[40] rises the stability difference between the two isomers of complex **2a** from 6.9 to 9.0 kcal mol^{-1} (**A** remaining the most stable). Also, for comparison, geometry optimizations of the two isomers of **2a** were performed with the M06 functional leading to same conclusions and a stability difference of 6.1 kcal mol^{-1}. The M06 functional is a hybrid meta-GGA functional developped by Truhlar and Zhao,[41] and it was shown to perform very well for transition metal systems, providing a good description of weak and long range interactions.[42]

Acknowledgement. Financial support by the Austrian Science Fund (FWF) is gratefully acknowledged (Project No. P24202-N17) and LFV ackowledges Fundação para a Ciência e Tecnologia, Projecto Estratégico - PEst-OE/QUI/UI0100/2013. The X-ray center of the Vienna University of Technology is acknowledged for financial support and for providing access to the single-crystal diffractometer.

Figure captions

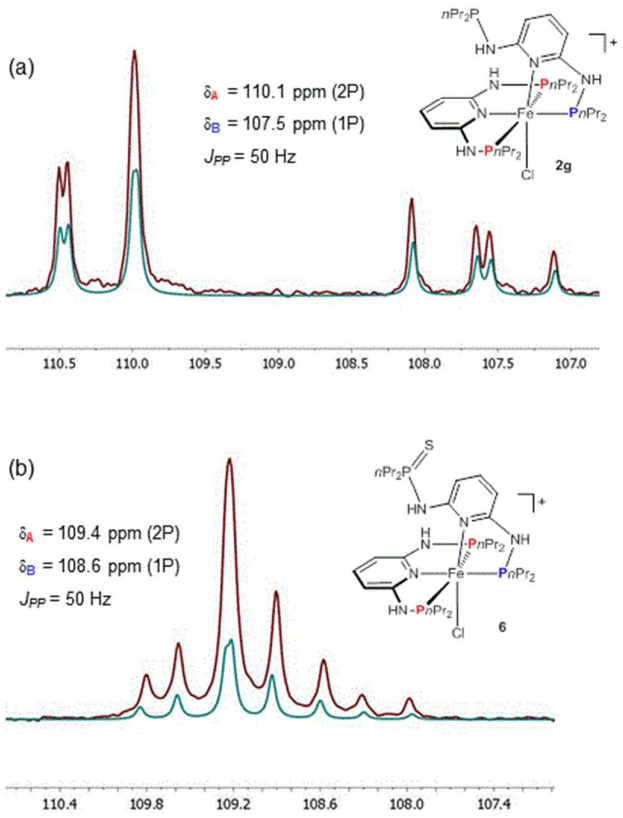

Figure 1. Experimental (red) and simulated (blue) $^{31}P\{^{1}H\}$ NMR spectra of **2g** and **6** (A_2B spin system, signal of the pendant P*n*Pr$_2$NH- and S=P*n*Pr$_2$NH- arms not shown).

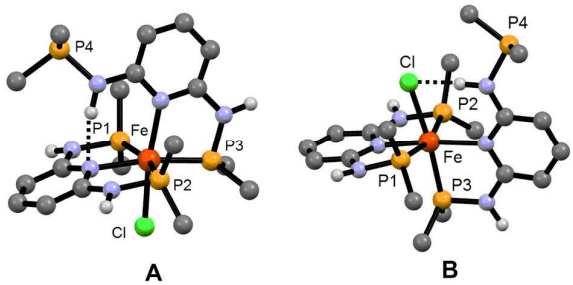

Figure 2. Optimized B3LYP geometries of the two possible isomers **A** and **B** of [Fe(κ^3-*P,N,P*-PNP-Ph)(κ^2-*P,N*-PNP-Ph)Cl]$^+$ (**2a**). Most hydrogen atoms are omitted and only *ipso* carbon atoms of the Ph substituents are shown for clarity.

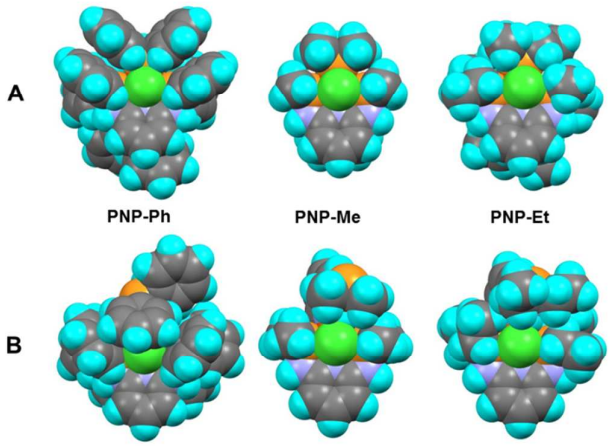

Figure 3. Space filling representation of optimized B3LYP geometries of the two possible isomers **A** and **B** of **2a** (Ph), **2c** (Me) **2d** (Et), and viewed along the Fe-Cl bond to illustrate steric crowding around the Cl ligand (green).

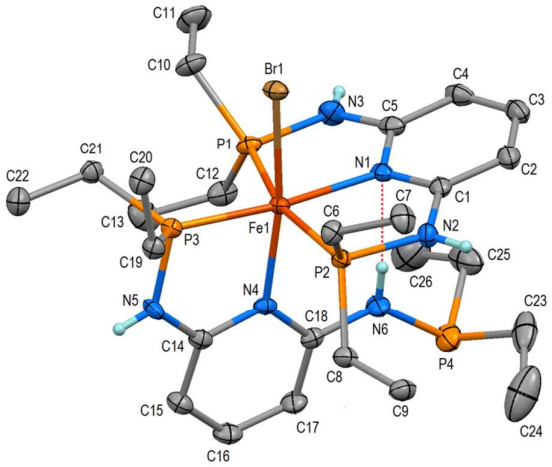

Figure 4. Structural view of [Fe(κ^3-P,N,P-PNP-Et)(κ^2-P,N-PNP-Et)Br]BPh$^{Me}_4$·3THF (**2f**BPh$^{Me}_4$·3THF) showing 50% thermal ellipsoids (most H-atoms, solvents and BPh$^{Me}_4^-$ omitted for clarity). Selected bond lengths (Å) and bond angles (deg): Fe(1)-P(1) 2.243(1), Fe(1)-P(2) 2.2521(9), Fe(1)-P(3) 2.189(1), Fe(1)-N(1) 2.063(2), Fe(1)-N(4) 2.117(2), Fe(1)-Br(1) 2.4878(9), P(1)-Fe(1)-P(2) 163.98(3), N(1)-Fe(1)-P(3) 171.38(6), Br(1)-Fe(1)-N(4) 171.03(6).

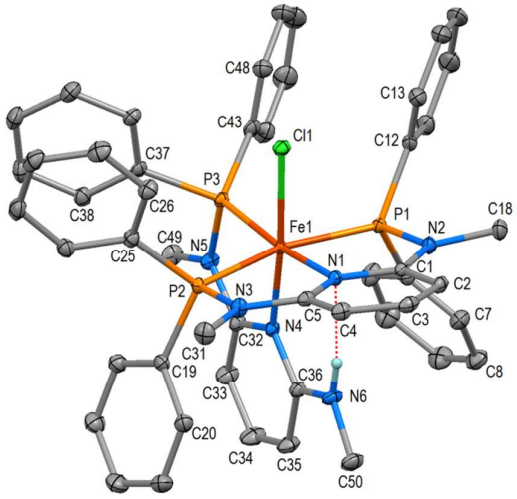

Figure 5. Structural view of [Fe(κ^3-P,N,P-PNP^{Me}-Ph)(κ^2-P,N-PN^{NHMe}-Ph)Cl]BF_4 (**3**) showing 50% thermal ellipsoids (most H-atoms and BF_4^- omitted for clarity). Selected bond lengths (Å) and bond angles (deg): Fe(1)-P(1) 2.2333(4), Fe(1)-P(2) 2.2410(4), Fe(1)-P(3) 2.1833(4), Fe(1)-N(1) 2.0472(9), Fe(1)-N(4) 2.0668(9), Fe(1)-Cl(1) 2.3323(3), P(1)-Fe(1)-P(2) 163.97(1), N(1)-Fe(1)-P(3) 171.60(3), Cl(1)-Fe(1)-N(4) 173.32(3).

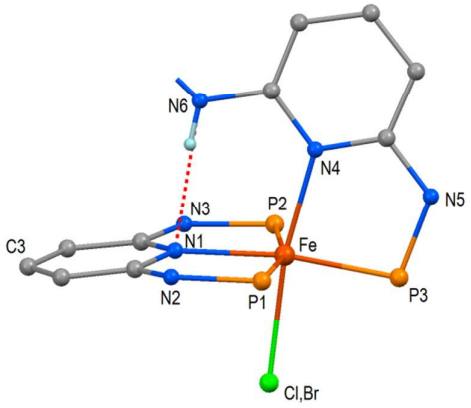

distances	mean	range [Å]
Fe - P1,P2	2.244	(2.234 - 2.253)
Fe - P3	2.186	(2.183 - 2.190)
Fe - N1	2.059	(2.047 - 2.065)
Fe - N4	2.096	(2.067 - 2.117)
Fe - Cl	2.338	(2.332 - 2.350)
N6...N1	2.889	(2.802 - 2.941)
angles	**mean**	**range [deg.]**
P1-Fe-P2	163.8	(163.3 - 164.0)
N1-Fe-P3	171.1	(170.0 - 171.6)
N1-Fe-Cl,Br	83.3	(81.4 - 84.9)
N1-Fe-N4	104.7	(104.0 - 105.9)
N4-Fe-Cl,Br	171.8	(170.5 - 173.3)
C3-N1-Fe	170.3	(166.0 - 172.9)

Figure 6. Representation of the complex cores of four [Fe(κ^3-PNP)(κ^2-PN(P))(Cl,Br)]-type complexes in compounds, **2a**BF_4·2THF·Et_2O,[15] **2e**BPh^{Me}_4·3THF, **2f**BPh^{Me}_4·3THF, and **3** and with mean values and ranges of bond lengths and bond angles. The red dotted line indicates a N-H···N hydrogen bond.

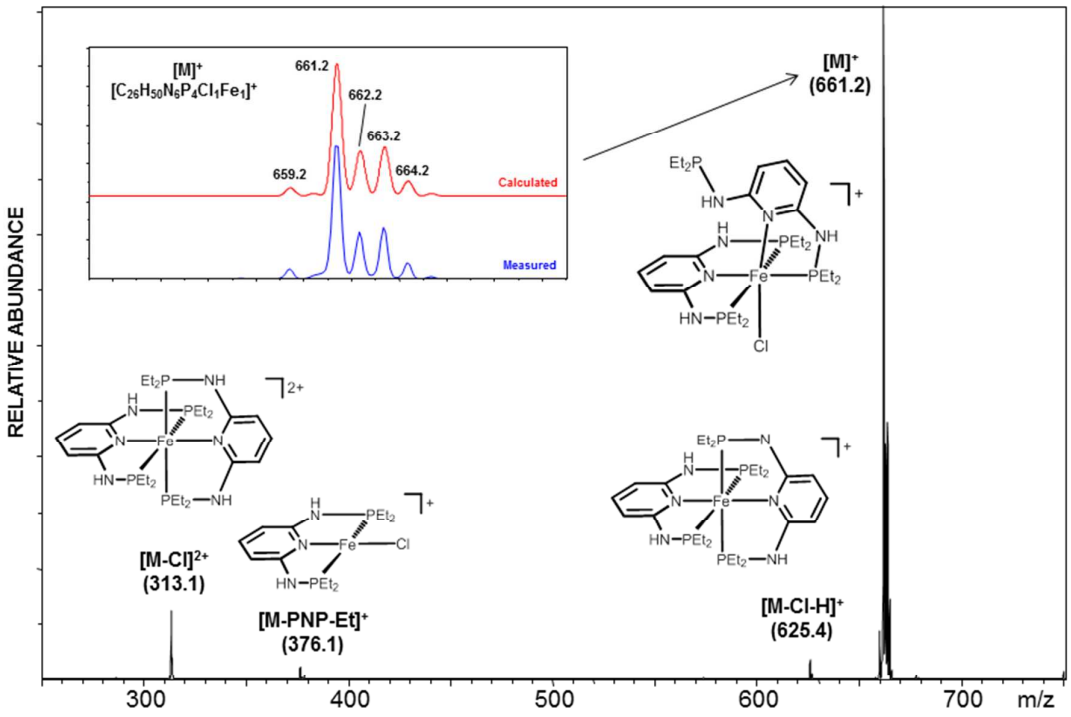

Figure 7. Positive-ion full scan ESI-MS of [Fe(κ^3-*P,N,P*-PNP-Et)(κ^2-*P,N*-PNP-Et)Cl]Cl (**2e**Cl) in CH_3OH. Inset shows the isotope pattern match for **2e**Cl ($[M]^+$).

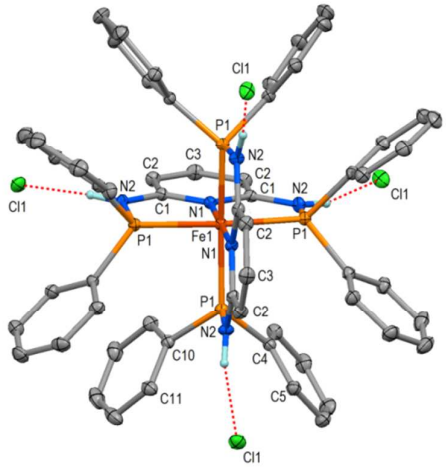

Figure 8. Structural diagram of [Fe(κ^3-*P,N,P*-PNP-Ph)$_2$](Cl)$_2$·solv (**5a**Cl·solv) showing only N-bonded H-atoms and 40%-ellipsoids. The complex has point symmetry -4 (S_4) with C3-N1-Fe1-N1-C3 as axial direction. Selected bond distances and angles (Å, deg): Fe1-N1 1.9563(12) (2x), Fe1-P1 2.2520(3) (4x); N1-Fe1-N1 180.0, N1-Fe1-P1 84.47(1) (4x), P1-Fe1-P1 168.93(1) (2x); hydrogen bond N2···Cl1 3.140(1) (4x).

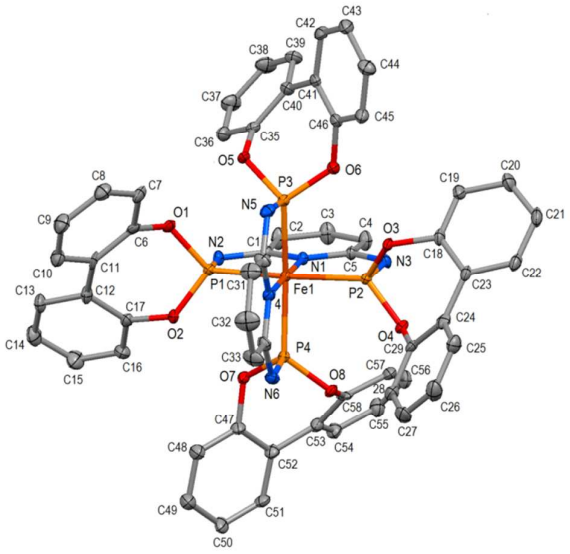

Figure 9. Structural diagram of [Fe(κ^3-*P,N,P*-PNP-BIPOL)$_2$](CF_3SO_3)$_2$·6.5THF (**5b**CF_3SO_3·6.5THF) showing 50%-ellipsoids. Most H-atoms, BF_4 anions and THF solvent molecules omitted for clarity. Selected bond distances and angles (Å, deg): Fe1-N4 1.967(7), Fe1-N1 1.969(6), Fe1-P4 2.180(2), Fe1-P1 2.181(2), Fe1-P2 2.182(2), Fe1-P3 2.189(2), N1-Fe1-N4 179.2(3), P1-Fe1-P2 167.47(9), P3-Fe1-P4 167.45(9).

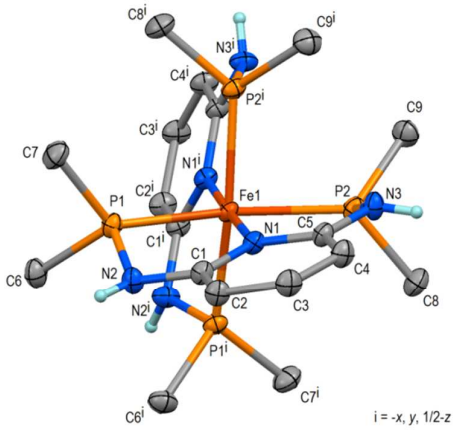

Figure 10. Structural view of [Fe(κ^3-*P,N,P*-PNP-Me)$_2$](CF_3SO_3)$_2$·2Me_2CO (**5c**CF_3SO_3·2Me_2CO) (most H-atoms, acetone solvent molecules and $CF_3SO_3^-$ omitted for clarity). Selected bond lengths (Å) and bond angles (deg): Fe(1)-P(1) 2.2748(5), Fe(1)-P(2) 2.2758(5), Fe(1)-N(1) 1.9973(14), P(1)-Fe(1)-P(2) 163.38(2) N(1)-Fe(1)-N(1) 178.23(9).

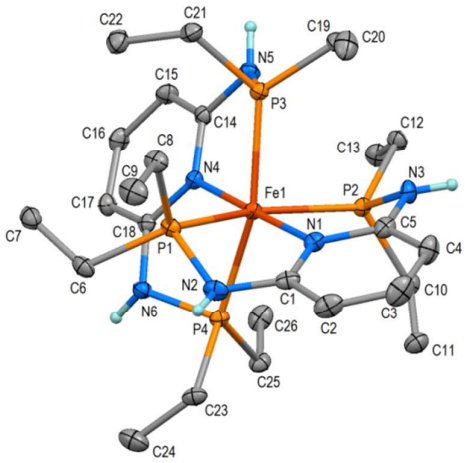

Figure 11. Structural view of [Fe(κ^3-*P,N,P*-PNP-Et)$_2$](BPh_4)$_2$·0.5Et_2O (**5d**BPh_4·0.5Et_2O) (most H-atoms, solvent and BPh_4^- omitted for clarity). Selected bond lengths (Å) and bond angles (deg): Fe(1)-P(1) 2.2804(4), Fe(1)-P(2) 2.2873(4), Fe(1)-P(3) 2.2898(6), Fe(1)-P(4) 2.3096(6), Fe(1)-N(1) 2.025(1), Fe(1)-N(4) 2.013(1), P(1)-Fe(1)-P(2) 157.93(2), P(3)-Fe(1)-P(4) 158.39(2).

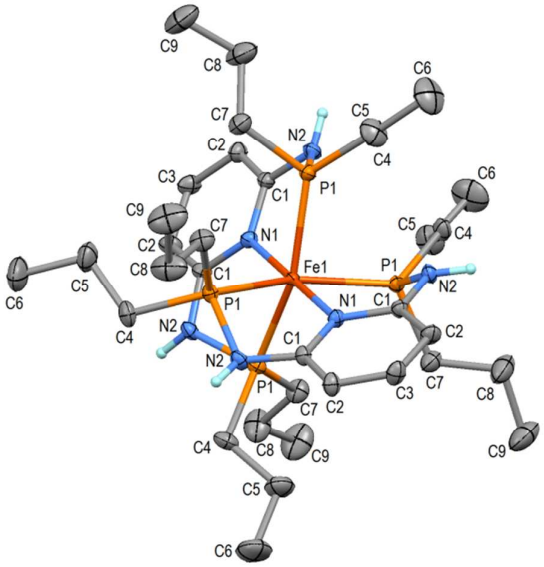

Figure 12. Structural view of [Fe(κ^3-*P,N,P*-PNP-*n*Pr)$_2$](BF$_4$)$_2$·2Me$_2$CO (**5e**BF$_4$·2Me$_2$CO) (most H-atoms, solvent and BF_4^- omitted for clarity). The complex has symmetry 222 (D_2) with Fe, N1, and C3 on one 2-fold axis. Selected bond lengths (Å) and bond angles (deg): Fe-N1 2.0317(13) (2×), Fe-P1 2.2740(3) (4×), N1-Fe-N1 180.0, *trans*-P1-Fe-P1 154.92(1) (2×).

References

1 For reviews on pincer complexes, see: (a) M. Albrecht and G. van Koten, *Angew. Chem., Int. Ed.* 2001, **40**, 3750. (b) M. E. van der Boom and D. Milstein, *Chem. Rev.* 2003, **103**, 1759. (c) J. T. Singleton, *Tetrahedron* 2003, **59**, 1837. (d) P. Bhattacharya and H. Guan, *Comment Inorg. Chem.* 2011, **32**, 88. (e) S. Schneider, J. Meiners and B. Askevold, *Eur. J. Inorg. Chem.* 2012, 412. (f) D. Morales-Morales and C. M. Jensen, Eds. The Chemistry of Pincer Compounds; Elsevier: Amsterdam, 2007. (g) D. Benito-Garagorri and K. Kirchner, *Acc. Chem. Res.* 2008, **41**, 201.

2 (a) B. L. Small, M. Brookhart, M. A. Bennett, *J. Am. Chem. Soc.* 1998, **120**, 4049. (b) Y. Chen, R. Chen, C. Qian, X. Dong and J. Sun, *Organometallics* 2003, **22**, 4312. (c) G. J. P. Britovsek, J. England, S. K. Spitzmesser, A. J. P. White and D. J. Williams, *Dalton Trans*. 2005, 945.

3 (a) G. J. P. Britovsek, V. C. Gibson, B. S. Kimberley, P. J. Maddox, S. J. McTavish, G. A. Solan, A. J. P. White and D. J. Williams, *Chem. Commun.* 1998, 849. (b) G. J. P. Britovsek, M. Bruce, V. C. Gibson, B. S. Kimberley, P. J. Maddox, S. Mastroianni, S. J. McTavish, C. Redshaw, G. A. Solan, S. Stromberg, A. J. P. White, D. J. Williams, *J. Am. Chem. Soc.* 1999, **121**, 8728.

4 S. C. Bart, E. Lobkovsky, P. J. Chirik, *J. Am. Chem. Soc.* 2004, **126**, 13749.

5 (a) W. V. Dahlhoff and S. M. Nelson, *J. Chem. Soc. (A)*, 1971, 2184. (b) P. Giannoccaro, G. Vasapollo, C. F. Nobile and A. Sacco, A. *Inorg. Chim. Acta.* 1982, **61**, 69. (c) G. Müller, M. Klinga, M. Leskelä and B. Rieger, *Z. Anorg. Allg. Chem.* 2002, **628**, 2839.

6 (a) J. Zhang, M. Gandelman, D. Herrman, G. Leitus, L. J. W. Shimon, Y. Ben-David and D. Milstein, *Inorg. Chim. Acta* 2006, **359**, 1955. (b) R. J. Trovitch, E. Lobkovsky and P. J. Chirik, *Inorg. Chem.* 2006, **45**, 7252.

7 E. M. Pelczar, T. J. Emge, K. Krogh-Jespersen and A. S. Goldman, *Organometallics* 2008, **27**, 5759.

8 (a) L. Zhang, D. Peng, X. Leng and Z. Huang, *Angew. Chem. Int. Ed.* 2013, **52**, 3676. (b) T. Zell, P. Milko, K. L. Fillman, Y. Diskin-Posner, T. Bendikov, M. A. Iron, G. Leitus, Y. Ben-David, M. L. Neidig and D. Milstein. *Chem. Eur. J.* 2014, **20**, 4403.

9 A. A. Danopoulos, N. Tsoureas, J. A. Wright and M. E. Light, *Organometallics* 2004, **23**, 166.

10 J. S. Judge, W. M. Reiff, G. M. Intille, P. Ballway and, W. A. Baker, Jr. *J. Inorg. Nuclear Chem.* 1967, **29**, 1711.

11 W.-S. W. DeRieux, A. Wong and Y. Schrodi, *J. Organomet. Chem.* 2014, **772-773**, 60.

12 (a) R. J. Trovitch, E. Lobkovsky, E. Bill and P. J. Chirik, *Organometallics* 2008, **27**, 1470. (b) S. K. Russell, J. M. Darmon, E. Lobkovsky and P. J. Chirik, *Inorg. Chem.* 2010, **49**, 2782.

13 (a) A. M. Tondreau, E. Lobkovsky, P. J. Chirik, Org. Lett. 2008, 10, 2789. (b) A. M. Tondreau, J. M. Darmon, B. M. Wile, S. K. Floyd, E. Lobkovsky and P. J. Chirik, *Organometallics* 2009, **28**, 3928. (c) A. M. Tondreau, C. C. H. Atienza, J. M. Darmon, C. Milsmann, H. M. Hoyt, K. J. Weller, S. A. Nye, K. M. Lewis, J. Boyer, J. G. P. Delis, E. Lobkovsky and P. J. Chirik, *Organometallics* 2012, **31**, 4886. (d) S. K. Russell, C. Milsmann, E. Lobkovsky, T. Weyhermüller´and P. J. Chirik, *Inorg. Chem*. 2011, **50**, 3159. (e) A. M. Tondreau, C. C. H.

Atienza, K. J. Weller, S. A. Nye, K. M. Lewis, J. G. P. Delis, and P. J. Chirik, *Science* 2012, **335**, 567.

14 (a) D. Benito-Garagorri, J. Wiedermann, M. Pollak, K. Mereiter and K. Kirchner, *Organometallics* 2007, **26**, 217. (b) D. Benito-Garagorri, M. Puchberger, K. Mereiter and K. Kirchner, *Angew. Chem., Int. Ed.*, 2008, **47**, 9142. (c) D. Benito-Garagorri, L. G. Alves, M. Puchberger, K. Mereiter, L. F. Veiros, M. J. Calhorda, M. D. Carvalho, L. P. Ferreira, M. Godinho and K. Kirchner, *Organometallics* 2009, **28**, 6902.

15 B. Bichler, M. Glatz, B. Stöger, K. Mereiter, L. F. Veiros and K. Kirchner, *Dalton Trans.* 2014, **43**, 14517.

16 S. R. M. M. de Aguiar, B. Stöger, E. Pittenauer, G. Allmaier, M. Puchberger, L. F. Veiros and K. Kirchner, *J. Organomet. Chem.* 2014, **760**, 74.

17 D. Benito-Garagorri, E. Becker, J. Wiedermann, W. Lackner, M. Pollak, K. Mereiter, J. Kisala and K. Kirchner, *Organometallics* 2006, **25**, 1900.

18 Ö. Öztopcu, C. Holzhacker, M. Puchberger, M. Weil, K. Mereiter, L. F. Veiros and K. Kirchner, *Organometallics* 2013, **32**, 3042.

19 T. E. Müller and D. M. P. Mingos, *Transition Met. Chem.* 1995, **20**, 533.

20 R. J. Abraham, J. Fisher and P. Loftus, Introduction to NMR Spectroscopy; John Wiley & Sons, Ltd.: New York, 1988.

21 (a) WI represents the Wiberg index. Wiberg indices are electronic parameters related with the electron density between two atoms, which scale as bond strength indicators. They can be obtained from a Natural Population Analysis. (b) K. B. Wiberg, *Tetrahedron* 1968, **24**, 1083;

22 S. Pavlik, K. Mereiter, M. Puchberger and K. Kirchner, *Organometallics* 2005, **24**, 3561.

23 P. Giannoccaro, G. Vasapollo, C. F. Nobile and A. Sacco, *Inorg. Chim. Acta.* 1982, **61**, 69.

24 D. D. Perrin and W. L. F. Armarego, *Purification of Laboratory Chemicals*, 3rd ed.; Pergamon: New York, 1988.

25 (a) S. K. Sur, *J. Magn. Reson.* 1989, **82**, 169. (b) D. F. Evans, *J. Chem. Soc.* 1959, 2003.

26 Computer programs APEX2, SMART, SAINT, SADABS, and SHELXTL (Bruker AXS Inc., Madison, WI, 2012).

27 G. M. Sheldrick *Acta Cryst.* 2008, **A64**, 112.

28 L. Palatinus and G. Chapuis, *J. Appl. Cryst.* 2007, **40**, 786.

29 V. Petříček, M. Dušek and L. Palatinus, 2006. JANA2006. Institute of Physics, Praha, Czech Republic.

30 C. F. Macrae, P. R. Edgington, P. McCabe, E. Pidcock, G. P. Shields, R. Taylor, M. Towler and J. van de Streek, *J. Appl. Cryst.* 2006, **39** 453.

31 A. L. Spek, *Acta Cryst.* 2009, **D65**, 148.

32 Gaussian 09, Revision A.02, M. J. Frisch, G. W. Trucks, H. B. Schlegel, G. E. Scuseria, M. A. Robb, J. R. Cheeseman, G. Scalmani, V. Barone, B. Mennucci, G. A. Petersson, H. Nakatsuji, M. Caricato, X. Li, H. P. Hratchian, A. F. Izmaylov, J. Bloino, G. Zheng, J. L. Sonnenberg, M. Hada, M. Ehara, K. Toyota, R. Fukuda, J. Hasegawa, M. Ishida, T. Nakajima, Y. Honda, O. Kitao, H. Nakai, T. Vreven, J. A. Montgomery, Jr., J. E. Peralta, F. Ogliaro, M. Bearpark, J. J.

Heyd, E. Brothers, K. N. Kudin, V. N. Staroverov, R. Kobayashi, J. Normand, K. Raghavachari, A. Rendell, J. C. Burant, S. S. Iyengar, J. Tomasi, M. Cossi, N. Rega, J. M. Millam, M. Klene, J. E. Knox, J. B. Cross, V. Bakken, C. Adamo, J. Jaramillo, R. Gomperts, R. E. Stratmann, O. Yazyev, A. J. Austin, R. Cammi, C. Pomelli, J. W. Ochterski, R. L. Martin, K. Morokuma, V. G. Zakrzewski, G. A. Voth, P. Salvador, J. J. Dannenberg, S. Dapprich, A. D. Daniels, Ö. Farkas, J. B. Foresman, J. V. Ortiz, J. Cioslowski, and D. J. Fox, Gaussian, Inc., Wallingford CT, 2009.

33 (a) A. D. Becke, *J. Chem. Phys.* 1993, **98**, 5648. (b) B. Miehlich, A. Savin, H. Stoll and H. Preuss, *Chem. Phys. Lett* 1989, **157**, 200. (c) C. Lee, W. Yang and G. Parr, *Phys. Rev. B* 1988, **37**, 785.

34 W. J. Hehre, L. Radom, P. v. R. Schleyer and J. A. Pople, *Ab Initio Molecular Orbital Theory*. John Wiley & Sons, New York, 1986.

35 R. G. Parr & W. Yang, in Density Functional Theory of Atoms and Molecules; Oxford University Press: New York, 1989.

36 (a) U. Haeusermann, M. Dolg, H. Stoll and H. Preuss, *Mol. Phys.* 1993, **78**, 1211; (b) W. Kuechle, M. Dolg, H. Stoll and H. Preuss, *J. Chem. Phys.* 1994, **100**, 7535; (c) T. Leininger, A. Nicklass, H. Stoll, M. Dolg and P. Schwerdtfeger, *J. Chem. Phys.* 1996, **105**, 1052.

37 (a) A. D. McLean and G. S. Chandler, *J. Chem. Phys.* 1980, **72**, 5639. (b) R. Krishnan, J. S. Binkley, R. Seeger and J. A. Pople, *J. Chem. Phys.* 1980, **72**, 650. (c) P. J. Hay, *J. Chem. Phys.* 1977, **66**, 4377. (d) K. Raghavachari and G. W. Trucks, *J. Chem. Phys.* 1989, **91**, 1062. (e) R. C. Binning and L. A. Curtiss, *J. Comput. Chem.* 1995, *10*3, 6104. (f) M. P. McGrath and L. Radom, *J. Chem. Phys.* 1991, **94**, 511.

38 (a) J. E. Carpenter and F. Weinhold, *J. Mol. Struct. (Theochem)* 1988, **169**, 41. (b) J. E. Carpenter, *PhD thesis*, University of Wisconsin (Madison WI), 1987. (c) J. P. Foster and F. Weinhold, *J. Am. Chem. Soc.* 1980, **102**, 7211. (d) A. E. Reed and F. Weinhold, *J. Chem. Phys.* 1983, **78**, 4066. (e) A. E. Reed and F. Weinhold, *J. Chem. Phys.* 1983, **78**, 1736. (f) A. E. Reed, R. B. Weinstock and F. Weinhold, *J. Chem. Phys.* 1985, **83**, 735. (g) A. E. Reed, L. A. Curtiss and F. Weinhold, *Chem. Rev.* 1988, **88**, 899. (h) F. Weinhold and J. E. Carpenter, *The Structure of Small Molecules and Ions*, Plenum, 1988, p. 227.

39 S. Grimme, J. Antony, S. Ehrlich and H. J. Krieg, *Chem. Phys.* 2010, **132**, 154104.

40 (a) A. D. Becke and E. R. J. Johnson, *Chem. Phys.* 2005, **122**, 154101. (b) E. R. Johnson and A. D. Becke, *J. Chem. Phys.* 2005, **123**, 24101. (c) E. R. Johnson and A. D. Becke, *J. Chem. Phys.* 2006, **124**, 174104.

41 Y. Zhao and D. G. Truhlar, *Theor. Chem. Acc.*, 2008, **120**, 215.

42 (a) Y. Zhao and D. G. Truhlar, *Acc. Chem. Res.*, 2008, **41**, 157. (b) Y. Zhao and D. G. Truhlar, *Chem. Phys. Lett.*, 2011, **502**, 1.